Identification of the Genetic Basis for the Large-tailed Phenotypic Trait in Han Sheep Through Integrated mRNA and miRNA Analysis of Tail Fat Tissue Samples

Yang Guangli (yangguangli_502@hotmail.com)
College of Animal Science and Technology, Henan Agricultural University, 450002 Zhengzhou, China

Zhang Huan
Henan Agricultural University

Zhang Shuhong
Shangqiu Normal University

Li Zhiqiang
Shangqiu Normal University

Gao Fengyi
Shangqiu Normal University

Wang Guan
Shangqiu Normal University

Wang Qiankun
Shangqiu Normal University

Li Xiangyu
Shangqiu Normal University

Yan Yongfeng
Shangqiu Normal University

Li Ming
Henan Agricultural University

Research

Keywords: RNA-Sequencing, Genetic Basis, Fatty large-tailed phenotype, Integrated Analysis, Sheep

Posted Date: November 18th, 2020

DOI: https://doi.org/10.21203/rs.3.rs-107294/v1

Abstract

Background: While evolution has led certain breeds of sheep to exhibit large tails composed of fatty tissue, the genetic basis for this fatty large-tailed phenotypic trait remains to be defined in breeds of Han sheep. Here, we employed a high-throughput sequencing approach to identify mRNAs and microRNAs (miRNAs) that were differentially expressed in tail fat tissue samples from large-tailed Han (LTH) and small-tailed Han (STH) sheep in order to identify key genetic determinants of the large-tailed phenotype.

Results: In total, we identified 521 mRNAs (237 upregulated, 284 downregulated) and 14 miRNAs (6 upregulated, 8 downregulated) that were differentially expressed between these two sheep breeds. Predictive analytical database tools were subsequently utilized to identify 2,409 putative targets of these differentially expressed miRNAs (DEMs), including 65 which were among the list of differentially expressed genes (DEGs) identified in the present study. By specifically focusing on predicted DEM/DEG pairs with appropriate regulatory directionality, we identified *DIRF*, *HSD17B12*, *LPL*, *APOBR*, *INSIGI*, *THRSP*, *ACSL5*, *FAAH*, *ACSS2*, *APOA1*, *ACLY*, and *ACSM3* through mRNA analyses and *ACSL4*, *FTO*, *FGF8*, *IGF2*, *GNPDA2*, *LIPG*, *PRKAA2*, *ELOVL7*, *SOAT2*, and *SIRT1* through miRNA analyses as candidate genes which may regulate fat deposition and fatty acid metabolism in the adipose tissue from the tails of Han sheep.

Conclusion: Together, our data provide insight into the potential genetic basis for the large-tailed phenotype of LTH sheep, suggesting that it may be attributable to specific DEMs and DEGs that regulate one another and thereby control lipid metabolism. These data provide a basis for future research regarding the role of these genes in ovine tail fat deposition, and offer preliminary perspectives on the molecular mechanisms governing the fatty large-tailed phenotype in LTH sheep.

Background

Sheep (*Ovis aries*) are among the most common species of livestock raised globally, and are particularly prevalent in China. Owing to the diverse climatic, ecological, and geographical conditions throughout China, sustained natural selection and selective breeding have led to the emergence of a wide array of indigenous Chinese sheep breeds [1]. Sheep are classified into five categories based their tail phenotype as follows: short-fat-tailed (Mongolian, Small-tailed Han), short thin-tailed (Tibetan), fat-rumped (Kazakh), long fat-tailed (Large-tailed Han), and long thin-tailed (Texel). Wild ancestors of sheep exhibited a thin-tailed phenotype, indicating that the fatty large-tailed phenotype emerged following domestication.

Adipose tissue is a major endocrine organ that plays a key role in energy storage, bat levels and locations of fat deposition vary dramatically between individuals and breeds. Genetic factors influencing these differences have been identified in pig [2], cattle [3], and human [4]. The specific genetic basis for tail fat deposition in sheep may be distinct from that governing intramuscular, kidney, and cardiac fat deposition, as tail fat serves as a primary energy reserve during periods of drought and famine in these animals.

Multiple genomic regions liked to tail fat deposition have been identified in breeds of Iranian sheep [5]. Moioli et al [6] have also employed a genome-wide analytical approach which enabled them to identify genomic regions and functional genes influencing ovine tail fat deposition. We have also utilized Ovine HD SNP chips to identify 8 quantitative trait loci associated with difference in tail fat deposition in Large-tailed Han (LTH) and Small-tailed Han (STH) breeds of sheep through a range of statistical analyses (unpublished). Sample-size-weighted fixed-effects genome-wide association (GWA) meta-analyses have further been used to clarify the genetic factors which influence body fat deposition [4]. Recently, RNA sequencing has been employed as a means of assessing genome-wide transcriptomic activity and can be used to complement GWA analyses of complex traits [7]. In addition, microRNAs (miRNAs) can post-transcriptionally suppress mRNA expression, thereby further regulating phenotypes of interest [8]. Several studies have employed RNA sequencing strategies to clarify functional genes and gene networks regulating complex traits in humans [9], cattle [3], pigs [4, 10-12], and mice [13].

In an effort to identify genes linked to ovine tail fat deposition, Wang et al. (2014) analyzed the adipose tissue transcriptome of Kazak and Tibetan sheep breeds [14], while Miao et al. (2015) conducted genome-wide analyses of mRNA and miRNA expression in STH and Dorset breeds to elucidate the genetic basis for phenotypic differences between these breeds [15,16]. While informative, these prior sequencing studies have focused on a limited number of animals and have not assessed intrinsic within-group variability. Additionally, no prior studies have focused on integrative mRNA and miRNA expression profiling in the adipose tail tissue of LTH and STH sheep breeds. As such, in the present study, we employed a high-throughput sequencing approach to identify mRNA and miRNA that were differentially expressed in the tail adipose tissue of LTH and STH animals with extremely divergent tail phenotypes. We further identified specific differentially expressed genes and miRNAs (DEGs and DEMs respectively) linked to lipid metabolism, and performed an integrative analysis to elucidate the genetics basis for this large-tailed phenotype.

Methods

Animals sampling

In total, three unrelated adult LTH sheep and three unrelated adult STH sheep were selected from among domestic populations located in Jia county of Henan Province, China, and Cao county of Shandong Province, China. All experimental subjects were two-year-old rams and were fed from weaning until slaughter with corn and green hay, with free access to water. Animal were defined as being unrelated if they had not shared a common ancestor for a minimum of three generations. Within 30 minutes of slaughter, samples of tail adipose tissue were collected from all sheep, snap-frozen, and stored at −80 °C until analysis.

RNA isolation, library preparation, and sequencing

A mortar and pestle were used to crush frozen tail fat tissue samples, after which TRIzol (Invitrogen, USA) were used toextract RNA from these samples based on provided directions. A Bioanalyzer 2100

instrument (Agilent Technologies, CA, USA) with an RNA 6000 Nano kit (Agilent, UK) and agarose gel electrophoresis were then used to analyze RNA quantity and quality with high-quality RNA subsequently being used for library preparation. Briefly, libraries preparation for mRNA sequencing was conducted with a standard Illumina standard kit as per the TruSeq RNA SamplePrep Guide (Illumina). Sample mRNA was isolated using oligo-dT beads, after which thermal fragmentation was conducted. Next, random primers and a cDNA Synthesis Kit (Invitrogen) were used to prepare cDNA, which was then converted to yield double-stranded cDNA fragments. All library preparation and sequencing were conducted as per the protocols of the Illumina NextSeq500 instrument (Illumina, USA) in order to generate 75 bp pair-end reads. Small RNA libraries for each of these experimental animals were conducted as above, instead utilizing an Illumina Truseq Small RNA Preparation kit according to the provided instructions. Personalbio (Shanghai, China) performed all sequencing analyses.

The Illumina's Sequencing Control Studio software version (SCS v2.8) were used to obtain raw sequencing data, and base-calling was conducted via the Illumina Real-Time Analysis version 1.8.70 (RTA v1.8.70) software. Extracted sequencing reads were then analyzed.

Mapping, assembly, and annotation

Generated mRNA reads were first quality-checked and converted into FastQC sequence files, after which Trim Galore was utilized with default settings to remove all sequencing adaptors, poly-A tails, and poly-T tails such that only paired-end reads with both pairs > 100 bp were retained for subsequent analysis. Cleaned reads were then mapped against the ovine genome (Oar_v3.1) and the annotation database ENSEMBL with the TopHat v2.0.1 with Bowtie2 software [17,18]. Cufflinks v2.0.2 was used to assemble and quantify transcripts with a minimum alignment counts per locus [18,19].

Cleaned unique small RNA reads were obtained by first conducting quality control with the fastx toolkit (v0.0.13.2), after which Mirdeep2 was used map these reads to the ovine genome assembly (Oar_v3.1, released Sept. 20, 2012) [20]. GenBank and Rfam were then used to exclude corresponding non-coding RNA sequences, and remaining small RNA sequences were searched against the mature miRNAs in miRBase v. 17.0 [21] to identify known miRNAs. Only perfectly mached miRNAs that identical to known precursor or mature RNA sequences within miRBase were annotated as candidate miRNAs.

Differentially expressed gene identification

Gene expression was assessed in terms of reads per kilobase per million mapped reads (RPKM), and was adjusted via a scaling normalization approach [22], with only those genes that had an RPKM > 1 or < -1 in a minimum of one sequenced sample being considered for downstream analyses. DEG identification was conducted with DEseq [23] and Cuffdiff [24], with *P* values being adjusted to control a false discovery rate (FDR) at 0.05 [25]. DEGs were identified as gene with a minimum fold-change of 2 and an adjusted $P < 0.05$, and were subjected to hierarchical clustering using the heatmap function in the R Bioconductor package [26].

Identification of differentially expressed miRNAs and their target genes

DEMs were identified using the R DESeq package [23], with normalized miRNA expression level being used to compare differential miRNAs expression levels between the generated libraries. Those miRNAs exhibiting a normalized read count of < 5 transcripts per million (TPM) in all libraries were not included in downstream analysis. DEMs were identified as those miRNAs with a greater than two-fold change in expression between groups that were significant as per the methods defined by Audic et al. (1997) method [27]. Putative DEM target genes were then identified using miRanda [28].

GO and KEGG analysis

DEG and DEM target gene enrichment in specific gene ontology (GO) categories was assessed using WEGO (Web GO) to assess enrichment for specific cellular component, molecular functions, and biological processes [29, 30], with numbers of genes associated with specific GO terms [31] and Kyoto Encyclopedia of Genes and Genomes (KEGG) pathways [32, 33] being quantified. The significance threshold for GO and KEGG enrichment analyses was $P < 0.05$.

Integrative DGG and DEM target genes analysis

Correlation between the expression of DEGs and DEMs were conducted in order to analyze four possible directional relationships (both upregulated, both downregulated, upregulated DEMs and downregulated DEGs, and downregulated DEMs and upregulated DEGs). For individual DEMs, analyses were conducted to determine whether numbers of differentially regulated target target genes were higher than predicted by chance alone using lists of both upregulated and downregulated DEGs. DEM and DEG datasets were then integrated, with only DEGs that were negatively correlated with DEMs being considered as targets for downstream analyses.

Results

RNA-sequencing analysis results

After successfully constructing six transcriptome libraries for mRNA expression profiling. We obtained 36.61 and 33.86 million raw sequence reads for each LTH and STH sample, respectively (Table 1), with 96.88% (24.33/25.08 million reads) and 94.53% (19.22/20.24 million reads) of these reads, respectively, being uniquely aligned to the Oar_v3.1 sheep reference genome. Over 99% of these reads exhibited a QC-score >20 and mapping rates were very high, consistent with the reliability of our results. Even distributions of mapped reads to all chromosomes were observed, with over 98% of the bases in these mapped reads corresponding to mRNA (LTH: 98.2%; STH 99.63%).

In total, RNA sequencing yielded 44,582,440 (L1), 21,670,754 (L2), 43,891,310 (L3), 15,088,076 (S1), 42,549,998 (S2), and 44,334,664 (S3) paired-end reads for the six individuals sequenced LTH and STH sheep. After quality control and filtering of these reads, 444,37,680, 21,622,512, 43,776,088, 15,040,666, 42,442,906, and 44,092,952 valid reads were obtained from the indicated sheep (Table 1). These reads

were then mapped to the annotated ovine genome (Oar_v3.1), with 73.9%, 57.6%, 68.3%, 55.4%, 45.1%, and 75.4% of the reads in these six individual LTH and STH sheep having successfully mapped to the genome, including 72.9%, 61.4%, 64.8% in the LTH sheep group and 59.9%, 49.9%, and 69.3% in the STH group that had mapped to genes (Table 1).

An average of 16 million raw reads per library was obtained following miRNA library sequencing, yielding 12,248,962, 15,829,550, 16,172,015, 15,480,083, 12,823,610, and 12,314,699 clean reads that were successfully mapped to the sheep genome for the L1, L2, L3, S1, S2, and S3 libraries, respectively (Table 2). Of these cleaned reads, 27,123 and 27,072 from LTH and STH sheep, respectively, aligned to unique miRNA sequences (Table 2). Total and unique RNA frequency distributions are shown in Figure 1, revealing highly diverse size distribution mapping to the sheep genome (Fig. 2). Most reads were between 18 to 36 nucleotides-long reads, with 22 nucleotides-long reads being the most common, followed by 21, 23, and 32 nucleotides-long (Fig. 3), consistent with the typical length of miRNAs. Proportions of small non-coding RNAs expression levels in these samples are shown in Table 3. Of these RNAs, miRNAs were the most abundantly expressed in libraries from both LTH and STH sheep (mean = 72.8%; Fig. 1), whereas other RNAs including ribosomal RNAs (rRNAs), small nucleolar RNAs (snoRNAs), small nuclear RNAs (snRNAs), and transfer RNAs (tRNAs) comprised 27.2% of the total expressed reads. Repeat-associated RNAs made up just 3% of these unique tags, while 7% of these tags did not map to any small non-coding RNA databases or to the sheep genome.

While miRNA do not directly encode proteins, their expression levels can offer functional insights into their role as post-transcriptional regulators. As miRNA functionality is also dependent upon spatiotemporal expression of target mRNAs, we therefore conducted integrated analyses of mRNA and miRNA profiles for LTH and STH sheep. In total, we identified 132 miRNAs in the tail fat tissue of these sheep (Table 4), with an average of 130 known miRNAs per sample (range: 125-132). Maxium miRNAs numbers were detected in sheep S2, while the lowest number of miRNAs was detected in the sample from sheep L2.

Analysis of differentially expressed genes between STH and LTH sheep

We next utilized the Cuffdiff software to identify DEGs when comparing STH and LTH sheep samples [19]. In total, we detected 20,137 mRNAs that were expressed in these samples (RPKM>1), including the majority of annotated sheep reference genes (Additional file 1: Table S1). We then assessed correlation between gene expression profiles in different samples, revealing generally strong Pearson correlation coefficients (ranging from 0.724 - 0.916; Fig. 4). When selecting DEGs, STH sheep were treated as the control group and LTH sheep as the experimental group. Clustering analyses (Fig. 5A), volcano plots (Fig. 6) were used to identify DEGs that were up- and down-regulated in LTH sheep relative to STH sheep. In total, we detected 521 significant DEGs in tail adipose tissue samples from these sheep (Additional file 2: Table S2), of which 237 were up-regulated and 284 were down-regulated. Several to DEGs associated with fatty acid synthesis, including *ADIRF*, *HSD17B12*, *LPL*, *APOBR*, *INSIG1, THRSP*, *ACSL5*, *FAAH*, *ACSS2*, *APOA1*, *ACLY*, and *ACSM3*, were upregulated in LTH sheep, potentially explaining this phenotype.

Analysis of differentially expressed miRNAs and their target genes

Next, we quantified differential miRNA expression patterns in the tails of LTH and STH sheep in terms of reads per million (RPM) values. All miRNAs with an RPM>10 were annotated based upon mature miRNA sequences recorded in miRBase (release 18.0), leading to the identification of 143 mature miRNAs in these six tissue samples (Additional file 3: Table S3). All miRNAs with < 2 nucleotide substitutions outside of the seed region were considered to represent a single miRNA family for the purposes of calculating differential expression. When we assessed tail fat miRNA expression profiles for LTH and STH sheep (Fig. 5B), we detected 132 known miRNAs. Those miRNAs with an average PRM>10 and a fold change between groups of >1 or < -1 were then identified as DEMs. Relative to LTH samples, STH samples exhibited 14 DEMs (6 upregulated and 8 downregulated) (Additional file 4: Table S4). The putative targets of these DEMs were then identified using miRanda program [28], leading to the identification of 2,409 possible target genes (Additional file 5: Table S5). As such, these identified DEMs were associated multiple targets and a range of regulatory modules, with an average of 172 target genes per DEM (range: 14-357). Identified DEM target genes include those associated with carbohydrate metabolism, the formation of anatomical structures, morphogenesis, lipid metabolism, kinase activity, and immune and inflammatory responses. Identified DEM target genes related to lipid metabolism are *ACSL4*, *FTO*, *FGF8*, *IGF2*, *GNPDA2*, *LIPG*, *PRKAA2*, *ELOVL7*, *SOAT2*, and *SIRT1*.

GOanalysis and functional annotation of DEGs and DEM target genes

A GO analysis of DEGs (RPKM<0.01or |log2Ratio| ≥ 1) was next conducted, with the resultant enriched biological process, cellular component, and molecular function GO terms being summarized in Table S6 (Additional file 6). With respect to biological processes, these genes were highly enriched for genes associated with translation (*P*=3.29E-05) and lipid metabolic processes (*P*=9.97e-05). These DEGs were enriched for cellular component GO terms linked to the cytoplasm, extracellular region, extracellular space, and organelles, while enriched molecular function included various structural molecules or functional activities. Overall, the most significantly enriched GO terms included extracellular region (*P*=8.60E-11), external encapsulating structure (*P*=4.75E-08), and extracellular space (*P*= 4.1E-06).

To better understand the functional implications of DEM-mediated the target gene regulation, we focused on DEM target genes that were negatively correlated with corresponding DEMs and subjected these genes to a GO analysis (Additional file 7; Table S7). These target genes were significantly enriched in cell death processes (*P*=4.3E-09), and were also associated with carbohydrate metabolism, ligase activity, lipid metabolic processes, protein maturation, and response to stress.

KEGG pathway analysis of DEGs and DEM target genes

Next, we conducted a KEGG pathway analysis of DEGs and DEM target genes identified through the above pairwise comparisons, revealing them to cluster primarily into the metabolism, cellular processes, environmental information processing, human diseases, organismal system, and genetic information processing pathways (Additional file 8: Table S8, Additional file 9: Table S9). Many of the identified DEGs

were particularly enriched in the metabolism and human diseases pathways, when comparing LTH sheep samples with those from STH sheep, the top significantly enriched pathways included translation (*P*=3.4E-07), lipid metabolism (*P*=4.91E-04), infectious diseases (*P*=7.1E-09), cancers (*P*=6.0E-06), carbohydrate metabolism (*P*=8.4E-06), cardiovascular diseases (*P*=4.2E-07), and xenobiotic biodegradation and metabolism (*P*=1.6E-07) (Additional file 8: Table S8). Subsequent KEGG enrichment analysis of the 2,409 identified DEM target genes revealed them to be enriched in three metabolism-related pathways ($P < 0.05$), including biosynthesis of other secondary metabolites, folding, sorting and degradation, cardiovascular diseases, carbohydrate metabolism, and immune diseases (Additional file 9: Table S9).

Integrated analysis of DEGs and DEMs

As detailed above, we selected DEGs and DEMs using either FDR <10% or $|\log2Ratio| \geq 1$ as cut-off criteria, with miRanda being used to predict DEM target gene [28]. In total, 14 DEMs had sheep orthologues, including 6 that were upregulated (oar-miR-133, oar-miR-150, oar-miR-376c-3p, oar-miR-154a-3p, oar-miR-655-3p, and oar-miR-376a-5p) and 8 that were downregulated (oar-let-7i, oar-miR-221, oar-miR-30a-3p, oar-miR-381-3p, oar-miR-411a-5p, oar-miR-495-3p, oar-miR-543-3p, oar-miR-543-3p, and oar-miR-412-3p). As such, these miRNAs and their putative target were subjected to downstream analysis. In total, these 14 DEMs were associated with 2,409 target genes. We then conducted an integrated analysis of these DEMs, the expression of their target genes, DEGs, and correlations between these expression profiles in sheep tail adipose tissues. We identified 65 total miRNA-mRNA interaction pairs through these analyses DEMs and DEGs (Additional file 10: Table S10).

Discussion

Genetics play a major role in determining patterns of fat distribution in animals. LTH sheep are an indigenous sheep breed in China that exhibit a desirable fatty large-tailed phenotype. Such tail fat deposition may be linked to differences in metabolic activities, adipocyte size, or developmental factors. Indeed, tail adipose tissue develops at later those in renal or cardiac adipose reserves [34]. Adipose tissue expansion is closely linked to the efficient storage and release of fatty acids within adipocytes, but the genetic genetic basis for the fatty tail phenotype observed in LTH sheep remains to be defined. We therefor conducted an RNA sequencing-based transcriptomic analysis of mRNA and miRNA expression patterns in adipose tissues from the tail of six LTH and STH sheep.

First, we successfully sequenced six transcriptomeic libraries and obtained 36.61 and 33.86 million raw sequence reads for our different sample types (Table 1), with over 94% of these raw reads being uniquely aligned to the Oar_v3.1 sheep reference genome, and with very high mapping rates. Based on these metrics, our results were more reliable than those from prior studies of Kazak and Tibetan sheep [14] or Han and Dorset sheep [16]. We therefor concluded that our data provided sufficient coverage to permit downstream analyses, as an average of 30 million reads has been shown to provide >90% coverage of annotated genes in yeast [35], chicken [36], and cattle [37]. These result were in line with those of prior

studies of other sheep breeds [14,16]. In miRNAs, an average of 16 million raw reads per library was obtained (Table 2). Raw reads after quality control, and these cleaned reads aligned to unique miRNA sequences (Table 2). RNA size distributions and mapping to the sheep genome are shown in Figure 1 and 2. Most reads were between 18 to 36 nucleotides-long reads (Fig. 3). Proportions of small non-coding RNAs expression levels in these samples are shown in Table 3. Of these RNAs, miRNAs were the most abundantly expressed in libraries from both LTH and STH sheep. While miRNA do not directly encode proteins, their expression levels can offer functional insights into their role as post-transcriptional regulators. We therefore identified 132 miRNAs in the tail fat tissue of these sheep (Table 4). Miao et al. (2015) previously identified 3,132 miRNAs in the adipose tissue of STH and Dorset sheep via RNA-sequencing [15]. In contrast, we identified significantly fewer miRNA in the present study (Additional file 3: Table S3), potentially due to differences in breeds, sequencing depth, and/or filtering criteria.

When selecting DEGs, STH sheep were treated as the control group and LTH sheep as the experimental group. In total, we detected 20,137 mRNAs that were expressed in these samples (Additional file 1: Table S1), and of these mRNAs, 521 significant DEGs were found in tail adipose tissue samples from these sheep (Additional file 2: Table S2), of which 237 were up-regulated and 284 were down-regulated. Clustering analyses (Fig. 5A) and volcano plots (Fig. 6) were used to identify DEGs that were up- and down-regulated in LTH sheep relative to STH sheep. In a prior study of Kazak and Tibetan sheep, authors identified 646 DEGs including 280 and 366 that were up-and down-regulated, respectively [14]. Miao et al. (2015) similarly identified 602 DEGs when comparing samples from STH and Dorset sheep [16]. As such, we detected fewer DEGs than in these prior studies (Additional file 2: Table S2), suggesting that distinct regulatory mechanisms govern adipogenesis in these different breeds.

In our identified DEGs, such as *ADIRF* (*Adipogenesis Regulatory Factor*) encodes a protein that is closely linked to adipocytic differentiation and development, controlling transcription activity early during the preadipocyte differentiation process [38, 39]. *HSD17B12* (*Hydroxysteroid 17-Beta dehydrogenase 12*) has been associated with suppressed adipocyte lipid accumulation, consistent with its predicted effect predicted in model system [40]. One key step in the energy metabolism process is the hydrolysis of triacylglycerol-rich lipoproteins by lipoprotein lipase in the vascular endothelium, resulting in the release of fatty acids that can subsequently be metabolized or stored for future use. *APOBR* (*Apolipoprotein B receptor*) encodes a receptor expressed on macrophage that controls cellular fat and vitamin uptake [41, 42]. In normal weight humans, a single high fat meal increased both *APOBR* expression and lipid uptake in monocytes [43]. High blood lipid levels differentially regulate *APOBR* expression in human postprandial monocytes and macrophages and lead to foam cell formation [44]. *INSIG1*(*Insulin-induced gene 1*) is a transmembrane ER-associated protein that retains sterol regulatory element-binding transcription factors (*SREBFs*) in the ER, thus preventing them from undergoing proteolytic activation within the Golgi apparatus and thereby controlling lipid metabolism [45,46], *INSIG1* also influences human obesity-related hypertriglyceridemia [47]. *THRSP* (T*hyroid hormone-inducible hepatic protein*) plays a role in regulating fatty acid synthesis-related gene expression [48], and its bovine homolog has been linked to muscle fatty acid composition in cattle [49]. In mice, *ACSL5* (*Acyl-CoA synthetases 5*) regulated systemic energy metabolism such that the knockout of this gene can prevent the onset of obesity and insulin resistance

[50]. *DGAT2* (*Diacylgycerol acyltransferase 2*) is an essential catalyst of triglyceride biosynthesis, which is important given that excessive triglyceride accumulation within adipose tissues is a key facet of obesity [51]. Overexpression of *FAAH* (*Fatty acid amide hydrolase*) can suppress *DGAT2* expression and triglyceride synthesis, and these genes may interact with one another to influence adiposity [51]. *ACSS2* (*Acetyl-CoA synthetase short-chain family member 2*) codes for a cytosolic enzyme that catalyzes acetate activation for use in the context of lipid synthesis and energy production. Vysochan et al. (2017) found that *ACSS2* was able to convert glucose-derived carbon into acetate for the generation of cytosolic acetyl-CoA during lipid synthesis, which they found to be a key process in the replication of HCMV and in virus-induced lipogenesis [52]. ApoA-I/HDL levels have also been linked to decreased body weight and enhanced insulin sensitivity [53, 54], such that ApoA-I-deficient mice exhibited increased body weight and body fat levels as well as decreased weight loss during caloric restriction, at least in part due to impaired lipolysis [55, 56]. Berton et al. (2016) determined that *ACSM3* (*Acyl-CoA synthetase medium-chain family member 3*) was liked to lipid metabolism and fatty acid composition in Nellore cattle, thereby impacting key meat quality traits [57]. Microarray analyses conducted in mice have additionally revealed that genes associated with lipolysis, fatty acid metabolism, mitochondrial energy transduction, oxidation-reduction, insulin sensitivity, and skeletal system development are downregulated in animals fed a high fat diet, whereas genes related to extracellular matrix remodeling and inflammation, including *ACSM*, are upregulated in these animals [58]. *ACL* (*ATP citrate lyase*) function in the cytosol wherein it converts mitochondria-derived citrate into oxaloacetate and acetyl-CoA, which can then be leveraged to facilitate lipid synthesis and acetylation [59]. Zaidi et al. (2012) also determined that a lack of *ACLY* bolstered the *ACSS2*-dependent synthesis of lipids [60]. Adipocytes lacking *ACLY* expression in vivo accumulate lipids, produce higher levels of acetate-derived acetyl-CoA and malonyl-CoA, and exhibit distinct patterns of fatty acid content and synthesis [61]. These genes were associated with lipid metabolism and fatty acid synthesis, potentially explaining this phenotype. This suggests that DEGs linked to lipid synthesis and triglyceride hydrolysis may mediate the enanced accumulation of lipids within the tails of LTH sheep, highlighting these genes as important targets for further study.

We quantified differential miRNA expression patterns in the tails of LTH and STH sheep in terms of reads per million (RPM) values. 143 mature miRNAs were identified in these six tissue samples (Additional file 3: Table S3). We assessed tail fat miRNA expression profiles for LTH and STH sheep (Fig. 5B), and identified 132 known miRNAs. Relative to LTH samples, STH samples exhibited 14 DEMs (6 upregulated and 8 downregulated) (Additional file 4: Table S4), with 2,409 putative targets having been identified (Additional file 5: Table S5). We found that identified DEMs played a range of roles in controlling tail fat deposition, development, and metabolism. For example, the Let-7 family of miRNAs have been shown to control glucose metabolism and blood glucose levels in murine loss-of-function experiments, at least in part owing to its ability to regulate muscle insulin signaling [62]. We found that oar-let-7i was downregulated in the present study, suggesting that it may control lipid metabolism and fat deposition in sheep tails. Additionally, miR-133 antagonism in the context of muscle regeneration has been shown to enhance respiratory uncoupling, thermogenesis, and glucose uptake within muscle, in addition to improving overall glucose tolerance, energy expenditure, and diet-induced obesity resistance

[63]. Levels of mir-133 are decreased in mice that are exposed to cold, leading to *de novo* satellite cell-derived brown adipocyte generation [63]. We determined that oar-mir-133 was upregulated, highlighting it as another putative regulator of ovine tail fat accumulation. Stable miR-376a and miR-376c overexpression have been shown to slow growth and migratory activity *in vitro*, and both of these miRNAs are predicted to suppress *IGF1R*. Such suppression has been confirmed via luciferase reporter assay in melanoma cells [64]. miR-411 is a miR-379 family member encoded in the DLK-DIO3 region of human chromosome 14 [65]. Harafuji et al. (2013) determined that miR-411 exhibits differential expressed in FSHD myoblasts, suggesting it may function as a controller of myogenesis [66]. miR-221 and miR-222 are also associated with myogenesis and are necessary for fully myocyte differentiation [67]. We found oar-miR-221 to be differentially regulated in the present study, suggesting that it may serve as a regulator of ovine fat deposition. Lee et al. (2014) found that miR-543 and miR-590-3p directly suppressed AIMP3/p18 translation, thereby impairing the onset of senescence [68]. Formosa et al. (2014) further found that miR-154, miR-376a, miR-376c, miR-381, and miR-495 controlled metastatic prostate regulate cancer cells proliferation, apoptosis, migration, and invasion [69]. Additional research has identified miR-495 as an inhibitor of bone regeneration, gastric cancer cell migration, and invasion, potentially owing to its ability to target high-mobility group AT-Hook 2 [70, 71]. We identified oar-miR-150, oar-miR-30a-3p, oar-miR-543-3p, oar-miR-412-3p, and oar-miR-154a-3p as DEMs in the present study, suggesting that they may be important regulators of metabolic activity and tail fat deposition in sheep. Identified DEM target genes included genes associated with carbohydrate metabolism, the formation of anatomical structures, morphogenesis, lipid metabolism, kinase activity, and immune/inflammatory responses. Overall, these results suggested that the identified DEMs may play central roles in the regulation of metabolism-associated gene expression in the context of sheep tail fat deposition, with both DEGs and DEMs being closely linked to metabolic activities including lipid metabolism.

We additionally leveraged GO enrichment analyses to identify certain genes that were important DEM regulatory targets in the context of lipid metabolism. Of the identified DEMs, miR-133 was predicted to target the greatest number of lipid metabolism-related genes, including *ACSL4*, *FTO*, *FGF8*, *IGF2*, and *GNPDA2*. *ACSL4* is an essential regulator of fatty acid metabolism, and the expression of *ACSL4* is controlled by *PPARδ*-mediated regulatory [72]. Smemo et al. (2014) established IRX3 as a functional long-range target of obesity-associated FTO variants and a key regulator of overall body composition [73]. Lopez-Sanchez et al. (2015) also determined that miR-133 is an essential mediator of crosstalk between the Fgf8 and Bmp2 signaling pathway owing to its ability to regulate Fgf8/ERK signaling in the context of cardiac induction [74], in line with our identifiition of *Fgf8* as a miR-133 target genes. *IGF2* is a DEM target gene that has likely been subjected to recent selective pressure, given that most domestic European pigs selected for lean growth carry a particular *IGF2* allele that induces decreased fat deposition and increased muscle growth [75]. The *GNPDA2* (*glucosamine-6-phosphate deaminase 2*) gene is an allosteric enzyme responsible for catalyzing reversible D-glucosamine-6-phosphate conversion into D-fructose-6-phosphate and ammonium. *GNPDA2* gene variants have previously been linked to obesity susceptibility and body mass index [76], and human GWAS studies have supported these links [77]. *LIPG* (*Endothelial lipase*) is a phospholipase that can decrease plasma HDL cholesterol levels [78]. *ELOVL7* (*Elongation of very-long*

chain fatty acids protein 7) controls the elongation of C18:0, C20:0, and other very-long-chain fatty acids [79], with *in vitro* analyses having shown this gene to specifically control saturated very- long-chain fatty acids elongation [80]. Prior studies of pigs have identified *ELOVL7* as a candidate gene related fatty acid composition in porcine muscle and abdominal fat tissues [81], suggesting that it also warrants research to evaluate its impact on long-chain fatty acids in sheep. *PRKAA2* (*Protein Kinase AMP-Activated Catalytic Subunit Alpha 2*) encodes a catalytic subunit of the AMP-activated protein kinase (AMPK), which is a central regulator of cellular energy status, and involved in the glucose and lipid metabolism [82]. Lee et al. (2007) have investigated the porcine *PRKAA2* gene as a positional candidate regulator of intramuscular fat and backfat thickness traits in pig chromosome 6 [83]. *SOAT2* (*Sterol O-acyltransferase 2*), also known as *ACAT2*, encodes an enzyme that is primarily expressed in the intestine and liver and that controls cholesterol esterification, beta-oxidation, and lipid metabolism [84]. It serves as a key regulator of lipid and cholesterol metabolism in humans and cattle, and significantly *ACAT2* variability has been detected in samples of human liver tissue, indicating that it is associated with over half of ACAT activity in most humans [84]. In one study of broiler chickens, hepatic *ACAT2* expression was shown to regulate abdominal fat accumulation of [85]. Correlations between cholesterol and *ACAT2* have been reported in fish [86], and in human have been linked to increased lean mass [87]. ACAT2 has also been shown to regulate enzymes associated with lipogenesis and lipolysis in beef cattle and pigs [88, 89]. *SIRT1* (*sirtuin 1*) regulates lipid and glucose metabolism to control overall energy metabolism, and genetic research has been conducted to assess the impact of *SIRT1* SNPs on adiposity. In one case-control association study conducted in Belgium of 1,068 obese patients and 313 lean controls, *SIRT1* variants were linked to an increased risk of obesity and were correlated with visceral obesity-related parameters in obese males [90]. Both SNPs and overall *SIRT1* expression levels have also been linked to severe obesity [91]. Together, our results suggest that these DEMs and their target genes are likely to play ket roles in regulating sheep tail fat deposition and lipid metabolism.

Many of the genes enriched in the identified pathway were associated with lipid synthesis and metabolisms, with the majority also being associated with the fatty acid metabolism pathway. *SIRT1* has previously been identified as a key regulator of cellular differentiation, energy metabolism, and resistance to stress [92]. In total, we additionally identified 28 genes that were linked to adipogenesis and lipid metabolism in prior studies. Many of these genes were downregulated in tail fat tissue samples from LTH sheep relative to those from STH sheep, consistent with the hypothesis that lipid metabolic activities are decreased in tail adipocytes of LTH sheep. In addition, we found that certain tail fat deposition-related genes (*FASN*, *FABP4*, *LPL*, *THRSP*, and *DGAT1*) were also downregulated in the tail fat of these animals. These patterns of gene expression were distinct from those in similar prior studies, and emphasize the importance of conducting further research to better understand the degree to which these differences are attributable to breed-specific differences. Additionally, it may be beneficial to evaluate the functional relevance of tail fat deposition-related gene expression in different sheep breed by grouping tail fat samples according to corresponding tail weight indices.

As detailed above, when we conducted an integrated analysis of these DEMs, the expression of their target genes, DEGs, and correlations between these expression profiles in sheep tail adipose tissues. We

identified 65 total miRNA-mRNA interaction pairs through these analyses DEMs and DEGs (Additional file 10: Table S10). Given the large number of target genes identified, it is likely that this small set of DEMs can regulate the expression of many important genes in the context of tail fat deposition. miRNAs are short non-coding RNAs that post-transcriptionally regulate gene expression. They generally bind to complementary sequence in the 3'- untranslated region (UTR) of their target mRNAs and repress protein production via translational silencing and mRNA destabilization [93]. In addition, long noncoding RNAs (lncRNAs) can additionally function as transcriptional regulators by binging to histone-modifying complexes, DNA binding proteins, and even to RNA polymerase II, thereby modulatin gene expression [94]. While we identified 14 relevant DEMs and 521 DEGs in this study, relatively few interaction pairs were identified based on these sequencing data. Differences obtained when using different DEG lists suggest that the miRNA control mRNA expression in a carefully regulated manner.

Conclusions

In summary, in the present study, we conducted an integrated analysis of mRNA and miRNA expression patterns in tail adipose tissue from LTH and STH sheep, leading to the identification of DEGs and DEMs that were highly expressed in LTH tissue samples relative to STH samples. These DEGs and DEMs were predicted to play key functional and regulatory roles in the regulation of deposition and metabolic activation in the tails of LTH sheep. Overall, these data provide a foundation for further studies of the biological roles of these DEGs, DEMs, and DEM target genes in the context of ovine tail fat deposition, highlighting potential mechanisms governing this fatty large-tailed phenotypic trait.

Declarations

Acknowledgments

This study was supported by the He'nan Research Program of Foundation and Advanced Technology of China (102300410143, 132300410398), the Foundation of He'nan Educational Committee of China (12B230011, 14B230017), and the Cooperation Project of Henan Science and Technology Department of China (182107000041).

Authors' contributions

GLY and ML conceived and designed the project. QKW, XYL, and YFY collected the samples. HZ, ZQL, FYG, and GW extracted the RNA. GLY, HZ, and SHZ analyzed the data, and wrote the paper. All authors reviewed and approved the manuscript.

Competing interests

The authors declare that they have no competing interests.

Ethics approval and consent to participate

The experiment was approved by the Ministry of Science and Technology of China and the Ethics Committee of Shangqiu Normal University. All animal procedures were conducted according to the guidelines for the care and use of experimental animals established by the Ministry of Science and Technology of China (Guidelines on Ethical Treatment of Experimental Animals (2006) No. 398).

Availability of data and materials

The datasets used and analysed during this study are available on request from the corresponding author.

References

1. National Consultative Committee. Country Report for the Preparation of SoW-AnGR Report on Domestic Animal Genetic Resources in China. China Agriculture Press. 2004; Beijing, China.
2. Chen CY, Ai HS, Ren J, Li WB, Li PH, Qiao RM, et al. A global view of porcine transcriptome in three tissues from a full-sib pair with extreme phenotypes in growth and fat deposition by paired-end RNA sequencing. BMC Genomics. 2011; 12: 448.
3. Lee HJ, Jang M, Kim H, Kwak W, Park W, Hwang JY, et al. Comparative transcriptome analysis of adipose tissues reveals that ECM-receptor interaction is involved in the depot-specific adipogenesis in cattle. PLoS One. 2013;8: e66267.
4. Chu AY, Deng X, Fisher VA, Drong A, Zhang Y, Feitosa MF, et al. Multiethnic genome-wide meta-analysis of ectopic fat depots identifies loci associated with adipocyte development and differentiation. Nat Genet. 2017; 49:125–30.
5. Moradi MH, Nejati-Javaremi A, Moradi-Shahrbabak M, Dodds KG, McEwan JC. Genomic scan of selective sweeps in thin and fat tail sheep breeds for identifying of candidate regions associated with fat deposition. BMC Genet. 2012;13:10.
6. Moioli B, Pilla F, Ciani E. Signatures of selection identify loci associated with fat tail in sheep. J Anim Sci. 2015; 93: 4660–9.
7. Hekman JP, Johnson JL, Kukekova AV. Transcriptome analysis in domesticated species: challenges and strategies. Bioinform Biol Insights. 2016; 9(Suppl4): 21–31.
8. Williams MD, Mitchell GM. MicroRNAs in insulin resistance and obesity. Exp Diabetes Res. 2012; 2012:484696.
9. Parts L, Hedman ÅK, Keildson S, Knights AJ, Abreu-Goodger C, van de Bunt M, et al. Extent, causes, and consequences of small RNA expression variation in human adipose tissue. PLoS Genet. 2012; 8: e1002704.
10. Ramayo-Caldas Y, Mach N, Esteve-Codina A, Corominas J, Castelló A, Ballester M, et al. Liver transcriptome profile in pigs with extreme phenotypes of intramuscular fatty acid composition. BMC Genomics. 2012; 13: 547.

11. Ayuso M, Fernández A, Núñez Y, Benítez R, Isabel B, Barragán C, et al. Comparative analysis of muscle transcriptome between pig genotypes identifies genes and regulatory mechanisms associated to growth, fatness and metabolism. PLoS One. 2015;10: e0145162.
12. Pérez-Montarelo D, Madsen O, Alves E, Rodríguez MC, Folch JM, Noguera JL, et al. Identification of genes regulating growth and fatness traits in pig through hypothalamic transcriptome analysis. Physiol Genomics. 2013; 46:195–206.
13. Thomou T, Mori MA, Dreyfuss JM, Konishi M, Sakaguchi M, Wolfrum C, et al. Adipose-derived circulating miRNAs regulate gene expression in other tissues. Nature. 2017, 542: 450–5.
14. Wang XL, Zhou GX, Xu XC, Geng RQ, Zhou JP, Yang YX, et al. Transcriptome profile analysis of adipose tissues from fat and short-tailed sheep. Gene. 2014; 549: 252–7.
15. Miao XY, Luo QM, Qin XY, Guo YT. Genome-wide analysis of microRNAs identifies the lipid metabolism pathway to be a defining factor in adipose tissue from different sheep. Sci Rep. 2015; 5:18470.
16. Miao XY, Luo QM, Qin XY, Guo YT, Zhao HJ. Genome-wide mRNA-seq profiling reveals predominant down-regulation of lipid metabolic processes in adipose tissues of Small Tail Han than Dorset sheep. Biochem Bioph Res Co. 2015; 467: 413–20.
17. Trapnell C, Pachter L, Salzberg SL. TopHat: discovering splice junctions with RNA-Seq. Bioinformatics. 2009; 25:1105–11.
18. Trapnell C, Roberts A, Goff L, Pertea G, Kim D, Kelley DR, et al. Differential gene and transcript expression analysis of RNA-seq experiments with TopHat and Cufflinks. Nat Protoc. 2012; 7:562–78.
19. Trapnell C, Williams BA, Pertea G, Mortazavi A, Kwan G, van Baren MJ, et al. Transcript assembly and quantification by RNA-Seq reveals unannotated transcripts and isoform switching during cell differentiation. Nat Biotech. 2010; 28: 511–5.
20. Mackowiak SD. Identification of novel and known miRNAs in deep-sequencing data with miRDeep2. Curr Protoc Bioinformatics. 2011; Chapter 12: Unit 12.10.
21. Griffiths-Jones S. The microRNA Registry. Nucleic Acids Res. 2004; 32(Database issue): D109–11.
22. Robinson MD, Oshlack A. A scaling normalization method for differential expression analysis of RNA-seq data. Genome Biol. 2010;11: R25.
23. Anders S, Huber W. Differential expression analysis for sequence count data. Genome Biol. 2010; 11: R106.
24. Roberts A, Trapnell C, Donaghey J, Rinn JL, Pachter L. Improving RNA-Seq expression estimates by correcting for fragment bias. Genome Biol. 2011; 12, R22.
25. Benjamini Y, Hochberg Y. Controlling the false discovery rate: a practical and powerful approach to multiple testing. J R Stat Soc Series B Stat Methodol. 1995; 57:289–300.
26. Gentleman RC, Carey VJ, Bates DM, Bolstad B, Dettling M, Dudoit S, et al. Bioconductor: open software development for computational biology and bioinformatics. Genome Biol. 2004; 5: R80.

27. Audic S, Claverie JM. The significance of digital gene expression profiles. Genome Res.1997; 7: 986–95.
28. Enright AJ, John B, Gaul U, Tuschl T, Sander C, Marks DS. MicroRNA targets in Drosophila. Genome Biol. 2003; 5: R1.
29. Ashburner M, Ball CA, Blake JA, Botstein D, Butler H, Cherry JM, et al. Gene ontology: tool for the 54 unification of biology. The Gene Ontology Consortium. Nat Genet.2000; 25: 25–9.
30. Ye J, Fang L, Zheng H, Zhang Y, Chen J, Zhang Z, et al. WEGO: a web tool for plotting GO annotations. Nucleic Acids Res. 2006; 34: W293–7.
31. Harris MA, Clark J, Ireland A, Lomax J, Ashburner M, Foulger R, et al. The Gene Ontology (GO) database and informatics resource. Nucleic Acids Res. 2004; 32: D258–61.
32. Kanehisa M, Goto S, Kawashima S, Okuno Y, Hattori M. The KEGG resource for deciphering the genome. Nucleic Acids Res. 2004; 32: D277–80.
33. Kanehisa M, Goto S, Hattori M, Aoki-Kinoshita KF, Itoh M, Kawashima S, et al. From genomics to chemical genomics: new developments in KEGG. Nucleic Acids Res. 2006; 34: D354–7.
34. Yang GL, Liu KD, Fu HH, Feng G, Wang MC. Comparative study on adipocyte size of heart fat, renal fat, and tail fat in Large-tailed han sheep. Heilongjiang Animal Science and Veterinary Medicine, 2019, (19): 60–4, 179.
35. Nagalakshmi U, Wang Z, Waern K, Shou C, Raha D, Gerstein M, et al. The transcriptional landscape of the yeast genome defined by RNA sequencing. Science. 2008; 320: 1344–9.
36. Wang Y, Ghaffari N, Johnson CD, Braga-Neto UM, Wang H, Chen R, et al. Evaluation of the coverage and depth of transcriptome by RNA-Seq in chickens. BMC Bioinformatics. 2011; 12 Suppl 10: S5.
37. Li RW, Rinaldi M, Capuco AV. Characterization of the abomasal transcriptome for mechanisms of resistance to gastrointestinal nematodes in cattle. Vet Res. 2011; 42: 114.
38. Ni Y, Ji C, Wang B, Qiu J, Wang J, Guo X. A Novel pro-adipogenesis factor abundant in adipose tissues and over-expressed in obesity acts upstream of PPARgamma and C/EBPalpha. J. Bioenerg. Biomembr.2013; 45:219–28.
39. Lee SJ, Blanchett-Anderson S, Keep SG, Gasche MB, Wang MM. Tripartite factors leading to molecular divergence between human and murine smooth muscle. PLoS One. 2020; 15(1): e0227672.
40. Söhle J, Machuy N, Smailbegovic E, Holtzmann U, Grönniger E, Wenck H, et al. Identification of new genes involved in human adipogenesis and fat storage. PLoS One. 2012; 7:e31193.
41. Brown ML, Ramprasad MP, Umeda PK, Tanaka A, Kobayashi Y, Watanabe T, et al. A macrophage receptor for apolipoprotein B48: cloning, expression, and atherosclerosis. Proc Natl Acad Sci USA. 2000; 97: 7488–93.
42. Brown ML, Yui K, Smith JD, LeBoeuf RC, Weng W, Umeda PK, et al. The murine macrophage apoB-48 receptor gene (Apob-48r): homology to the human receptor. J Lipid Res. 2002; 43: 1181–91.

43. Varela LM, Ortega-Gomez A, Lopez S, Abia R, Muriana FJ, Bermudez B. The effects of dietary fatty acids on the postprandial triglyceride-rich lipoprotein/apoB48 receptor axis in human monocyte/macrophage cells. J Nutr Biochem. 2013; 24: 2031–9.
44. Varela LM, Ortega A, Bermudez B, Lopez S, Pacheco YM, Villar J, et al. A high-fat meal promotes lipid-load and apolipoprotein B-48 receptor transcriptional activity in circulating monocytes. Am J Clin Nutr. 2011; 93: 918–25.
45. Yang T, Espenshade PJ, Wright ME, Yabe D, Gong Y, Aeber-sold R, et al. Crucial step in cholesterol homeostasis: sterols promote binding of SCAP to INSIG-1, a membrane protein that facilitates retention of SREBPs in ER. Cell. 2002; 110: 489–500.
46. Gong Y, Lee JN, Lee PC, Goldstein JL, Brown MS, Ye J. Sterol-regulated ubiquitination and degradation of Insig-1 creates a convergent mechanism for feedback control of cholesterol synthesis and uptake. Cell Metab. 2006; 3:15–24.
47. Smith EM, Zhang Y, Baye TM, Gawrieh S, Cole R, Blangero J, et al. INSIG1 influences obesity-related hypertriglyc-eridemia in humans. *J. Lipid Res*. 2010; 51: 701–8.
48. Colbert CL, Kim CW, Moon YA, Henry L, Palnitkar M, McKean WB, et al. Crystal structure of Spot 14, a modulator of fatty acid synthesis. Proc Nat Acad Sci USA. 2010; 107:18820–25.
49. Oh DY, Lee YS, la BM, Lee JY, Park YS, Lee JH, et al. Identification of exonic nucleotide variants of the thyroid hormone responsive protein gene associated with carcass traits and fatty acid composition in korean cattle. Asian-Australas J Anim Sci. 2014; 27: 1373–80.
50. Bowman TA, O'Keeffe KR, D'Aquila T, Yan QW, Griffin JD, Killion EA, et al. Acyl CoA synthetase 5 (ACSL5) ablation in mice increases energy expenditure and insulin sensitivity and delays fat absorption. Mol Metab. 2016; 5: 210–20.
51. Ning T, Zou Y, Yang M, Lu Q, Chen M, Liu W, et al. Genetic interaction of DGAT2 and FAAH in the development of human obesity. Endocrine. 2017; 56: 366–78.
52. Vysochan A, Sengupta A, Weljie AM, Alwine JC, Yu Y. ACSS2-mediated acetyl-CoA synthesis from acetate is necessary for human cytomegalovirus infection. Proc Natl Acad Sci USA. 2017; 114: E1528–35.
53. Peterson SJ, Drummond G, Kim DH, Li M, Kruger AL, Ikehara S, et al. L-4F treatment reduces adiposity, increases adiponectin levels, and improves insulin sensitivity in obese mice. J. Lipid Res. 2008; 49: 1658–69.
54. Ruan X, Li Z, Zhang Y, Yang L, Pan Y, Wang Z, et al. Apolipoprotein A-I possesses an anti-obesity effect associated with increase of energy expenditure and up-regulation of UCP1 in brown fat. J. Cell. Mol. Med. 2011; 15: 763–72.
55. Ferreira SR, Almeida-Pittito B. Japanese-Brazilian Diabetes Study Group. Reflection about Japanese immigration to Brazil under the light of body adiposity. Arq. Bras. Endocrinol. Metabol. 2009; 53: 175–82.
56. Han R, Lai R, Ding Q, Wang Z, Luo X, Zhang Y, et al. Apolipoprotein A-I stimulates AMP-activated protein kinase and improves glucose metabolism. Diabetologia. 2007; 50: 1960–8.

57. Berton MP, Fonseca LF, Gimenez DF, Utembergue BL, Cesar AS, Coutinho LL, et al. Gene expression profile of intramuscular muscle in Nellore cattle with extreme values of fatty acid. BMC Genomics. 2016;17:972.
58. Choi MS, Kim YJ, Kwon EY, Ryoo JY, Kim SR, Jung UJ. High-fat diet decreases energy expenditure and expression of genes controlling lipid metabolism, mitochondrial function and skeletal system development in the adipose tissue, along with increased expression of extracellular matrix remodelling-and inflammation-related genes. Br J Nutr. 2015; 113: 867–77.
59. Das S, Morvan F, Jourde B, Meier V, Kahle P, Brebbia P, et al. ATP citrate lyase improves mitochondrial function in skeletal muscle. Cell Metab. 2015; 21: 868–76.
60. Zaidi N, Royaux I, Swinnen JV, Smans K. ATP citrate lyase knockdown induces growth arrest and apoptosis through different cell- and environment-dependent mechanisms. Mol Cancer Ther. 2012; 11: 1925–35.
61. Zhao S, Torres A, Henry RA, Trefely S, Wallace M, Lee JV, et al. ATP-citrate lyase controls a glucose-to-acetate metabolic switch. Cell Rep. 2016;17(4):1037–52.
62. Zhu H, Shyh-Chang N, Segrè AV, Shinoda G, Shah SP, Einhorn WS, et al. The Lin28/let-7 axis regulates glucose metabolism. Cell. 2011; 147:81–94.
63. Yin H, Pasut A, Soleimani VD, Bentzinger CF, Antoun G, Thorn S, et al. MicroRNA-133 controls brown adipose determination in skeletal muscle satellite cells by targeting Prdm16. Cell Metab. 2013;17: 210–24.
64. Zehavi L, Avraham R, Barzilai A, Bar-Ilan D, Navon R, Sidi Y, et al. Silencing of a large microRNA cluster on human chromosome 14q32 in melanoma: biological effects of mir-376a and mir-376c on insulin growth factor 1 receptor. Molecular Cancer. 2012; 11:44.
65. Glazov EA, McWilliam S, Barris WC, Dalrymple BP: Origin, evolution, and biological role of miRNA cluster in DLK-DIO3 genomic region in placental mammals. Mol Biol Evol. 2008, 25: 939–48.
66. Harafuji N, Schneiderat P, Walter MC, Chen YW. miR-411 is up-regulated in FSHD myoblasts and suppresses myogenic factors. Orphanet J Rare Dis. 2013; 8: 55.
67. Cardinali B, Castellani L, Fasanaro P, Basso A, Alema S, Martelli F, et al. Microrna-221 and microrna-222 modulate differentiation and maturation of skeletal muscle cells. PLoS One 2009, 4:e7607.
68. Lee S, Yu KR, Ryu YS, Oh YS, Hong IS, Kim HS, et al. miR-543 and miR-590-3p regulate human mesenchymal stem cell aging via direct targeting of AIMP3/p18. Age (Dordr). 2014; 36: 9724.
69. Formosa A, Markert EK, Lena AM, Italiano D, Finazzi-Agro' E, Levine AJ, et al. MicroRNAs, miR-154, miR-299-5p, miR-376a, miR-376c, miR-377, miR-381, miR-487b, miR-485-3p, miR-495 and miR-654-3p, mapped to the 14q32.31 locus, regulate proliferation, apoptosis, migration and invasion in metastatic prostate cancer cells. Oncogene. 2014; 33:5173–82.
70. Tian Z, Zhou H, Xu Y, Bai J. MicroRNA-495 inhibits new bone regeneration via targeting high mobility group AT-hook 2 (*HMGA2*). Med Sci Monit. 2017; 23: 4689–98.
71. Wang H, Jiang Z, Chen H, Wu X, Xiang J, Peng J. MicroRNA-495 Inhibits gastric cancer cell migration and invasion possibly via targeting high mobility group AT-Hook 2 (*HMGA2*). Med Sci Monit. 2017;

23:640–8.

72. Kan CF, Singh AB, Dong B, Shende VR, Liu J. *PPARδ* activation induces hepatic long-chain acyl-CoA synthetase 4 expression in vivo and in vitro. Biochim Biophys Acta. 2015;1851:577–87.
73. Smemo S, Tena JJ, Kim KH, Gamazon ER, Sakabe NJ, Gómez-Marín C, et al. Obesity-associated variants within *FTO* form long-range functional connections with *IRX3*. Nature. 2014;507:371–5.
74. Lopez-Sanchez C, Franco D, Bonet F, Garcia-Lopez V, Aranega A, Garcia-Martinez V. Reciprocal repression between Fgf8 and miR-133 regulates cardiac induction through Bmp2 signaling. Data Brief. 2015; 5: 59–64.
75. Van Laere AS, Nguyen M, Braunschweig M, Nezer C, Collette C, Moreau L, et al. A regulatory mutation in *IGF2* causes a major QTL effect on muscle growth in the pig. Nature. 2003; 425:832–6.
76. Ng MC, Tam CH, So WY, Ho JS, Chan AW, Lee HM, et al. Implication of genetic variants near *NEGR1*, *SEC16B*, *TMEM18*, *ETV5/DGKG*, *GNPDA2*, *LIN7C/BDNF*, *MTCH2*, *BCDIN3D/FAIM2*, *SH2B1*, *FTO*, *MC4R*, and *KCTD15* with obesity and type 2 diabetes in 7705 Chinese. J Clin Endocrinol Metab. 2010; 95:2418–25.
77. Ouyang H, Zhang H, Li W, Liang S, Jebessa E, Abdalla BA, et al. Identification, expression and variation of the *GNPDA2* gene, and its association with body weight and fatness traits in chicken. PeerJ. 2016;4:e2129.
78. Jaye M, Lynch KJ, Krawiec J, Marchadier D, Maugeais C, Doan K, et al. A novel endothelial-derived lipase that modulates HDL metabolism. Nat Genet. 1999; 21: 424– 8.
79. Naganuma T, Sato Y, Sassa T, Ohno Y, Kihara A. Biochemical characterization of the very long-chain fatty acid elongase *ELOVL7*. FEBS Lett. 2011; 585: 3337–41.
80. Tamura K, Makino A, Hullin-Matsuda F, Kobayashi T, Furihata M, Chung S, et al. Novel lipogenic enzyme *ELOVL7* is involved in prostate cancer growth through saturated long-chain fatty acid metabolism. Cancer Res. 2009; 69:8133–40.
81. Yang B, Zhang W, Zhang Z, Fan Y, Xie X, Ai H, et al. Genome-wide association analyses for fatty acid composition in porcine muscle and abdominal fat tissues. PLoS One. 2013; 8: e65554.
82. Spencer-Jones NJ, Ge D, Snieder H, Perks U, Swaminathan R, Spector TD, et al. AMP-kinase alpha2 subunit gene *PRKAA2* variants are associated with total cholesterol, low-density lipoprotein-cholesterol and high-density lipoprotein-cholesterol in normal women. J Med Genet. 2006; 43:936–42.
83. Lee HY, Choi BH, Lee JS, Jang GW, Lee KT, Chung HY, et al. Molecular characterization and chromosomal mapping of the porcine AMP-activated protein kinase α2 *(PRKAA2*) gene. Asian Austral J Anim. 2007; 20(5): 615–21.
84. Parini P, Davis M, Lada AT, Erickson SK, Wright TL, Gustafsson U, et al. *ACAT2* is localized to hepatocytes and is the major cholesterol-esterifying enzyme in human liver. Circulation. 2004;110: 2017–23.
85. Wang X, Carre W, Rejto L, Cogburn LA. Transcriptional profiling in liver of hormonally-manipulated chickens. In: Dawson A, Sharp PJ, editors. Functional avian endocrinology. Narosa Publishing House,

2005, New Delhi, India.

86. Ushio H, Nagasaka R. Utilization of biological responses of fish and shellfish for improving seafood qualities. Aqua Bio Sci Mono. 2013; 6: 91–8.
87. Riechman SE, Andrews RD, Maclean DA, Sheather S. Statins and dietary and serum cholesterol are associated with increased lean mass following resistance training. J Gerontol A Biol Sci Med Sci. 2007; 62: 1164–71.
88. Jiang Z, Michal JJ, Chen J, Daniels TF, Kunej T, Garcia MD, et al. Discovery of novel genetic networks associated with 19 economically important traits in beef cattle. Int J Biol Sci. 2009, 5: 528–42.
89. Sodhi SS, Ghosh M, Song KD, Sharma N, Kim JH, Kim NE, et al. An approach to identify SNPs in the gene encoding acetyl-CoA acetyltransferase-2 (*ACAT-2*) and their proposed role in metabolic processes in pig. PLoS One. 2014; 9: e102432.
90. Peeters AV, Beckers S, Verrijken A, Mertens I, Roevens P, Peeters PJ, et al. Association of *SIRT1* gene variation with visceral obesity. Hum Genet. 2008; 124:431–6
91. Clark SJ, Falchi M, Olsson B, Jacobson P, Cauchi S, Balkau B, et al. Association of sirtuin 1 (*SIRT1*) gene SNPs and transcript expression levels with severe obesity. Obesity (Silver Spring). 2012; 20: 178–85.
92. Backesjo CM, Li Y, Lindgren U, Haldosen LA. Activation of *Sirt1* decreases adipocyte formation during osteoblast differentiation of mesenchymal stem cells. J Bone Miner Res. 2006; 21, 993–1002.
93. Jackson RJ, Standart N. How do microRNAs regulate gene expression? Biochem Soc Trans. 2008; 36, 1224–31.
94. Long Y, Wang X, Youmans DT, Cech TR. How do lncRNAs regulate transcription? Sci Adv, 2017; 3(9): eaao2110.

Figures

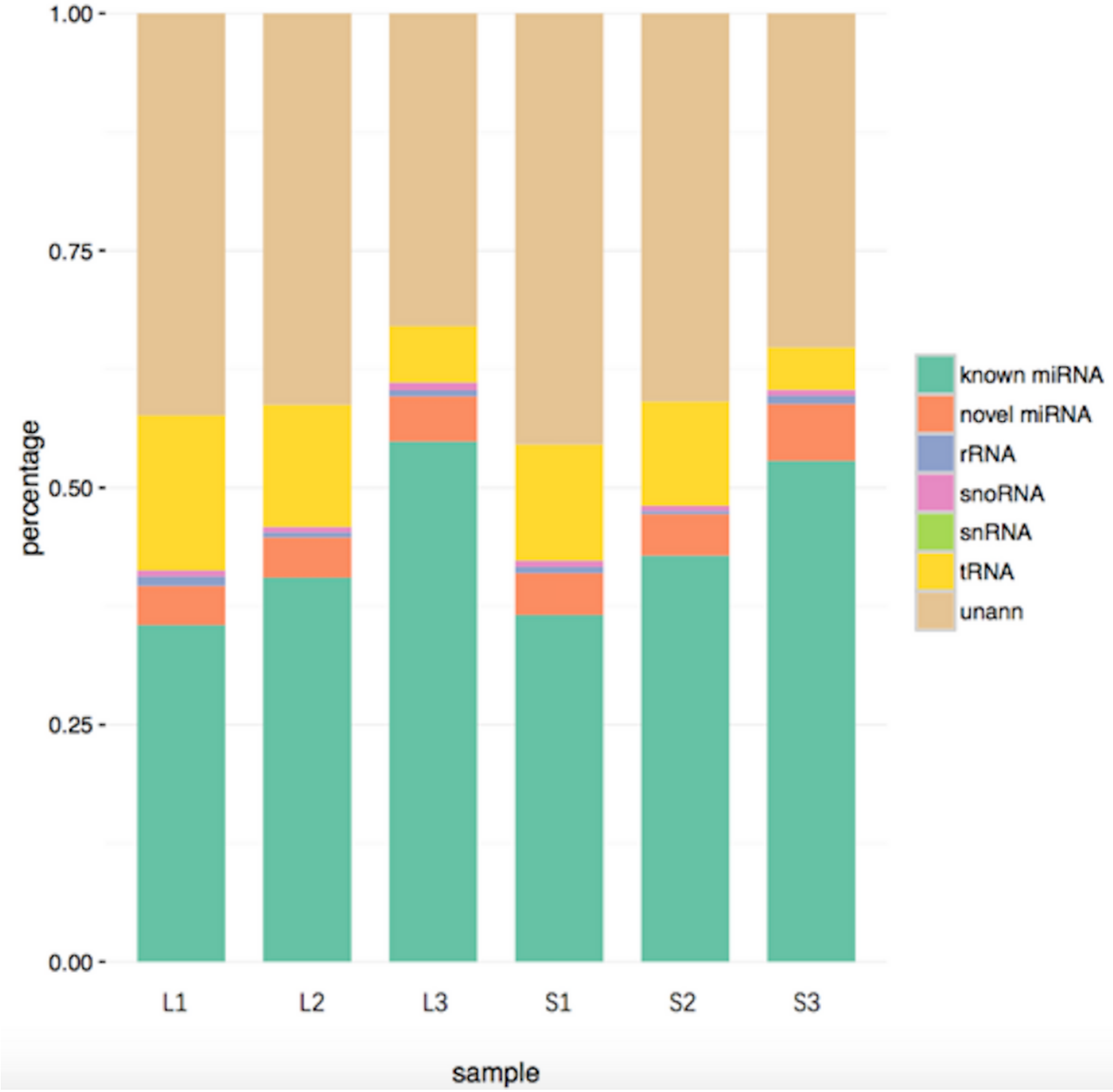

Figure 1

Frequency of small RNAs in tail fat tissues of the LTH and STH sheep breeds. The proportion of expressed adipose tissues small RNAs identical to LTH and STH sheep breed: i) the known miRNAs are shaded light green, ii) the novel miRNAs are shaded red, iii) repeat-associated RNA sequences are shaded blue (including rRNA, snoRNAs, and snRNAs), iv) tRNAs are shaded yellow, and v) the proportion of mapped but unclassified sequences is shaded brown.

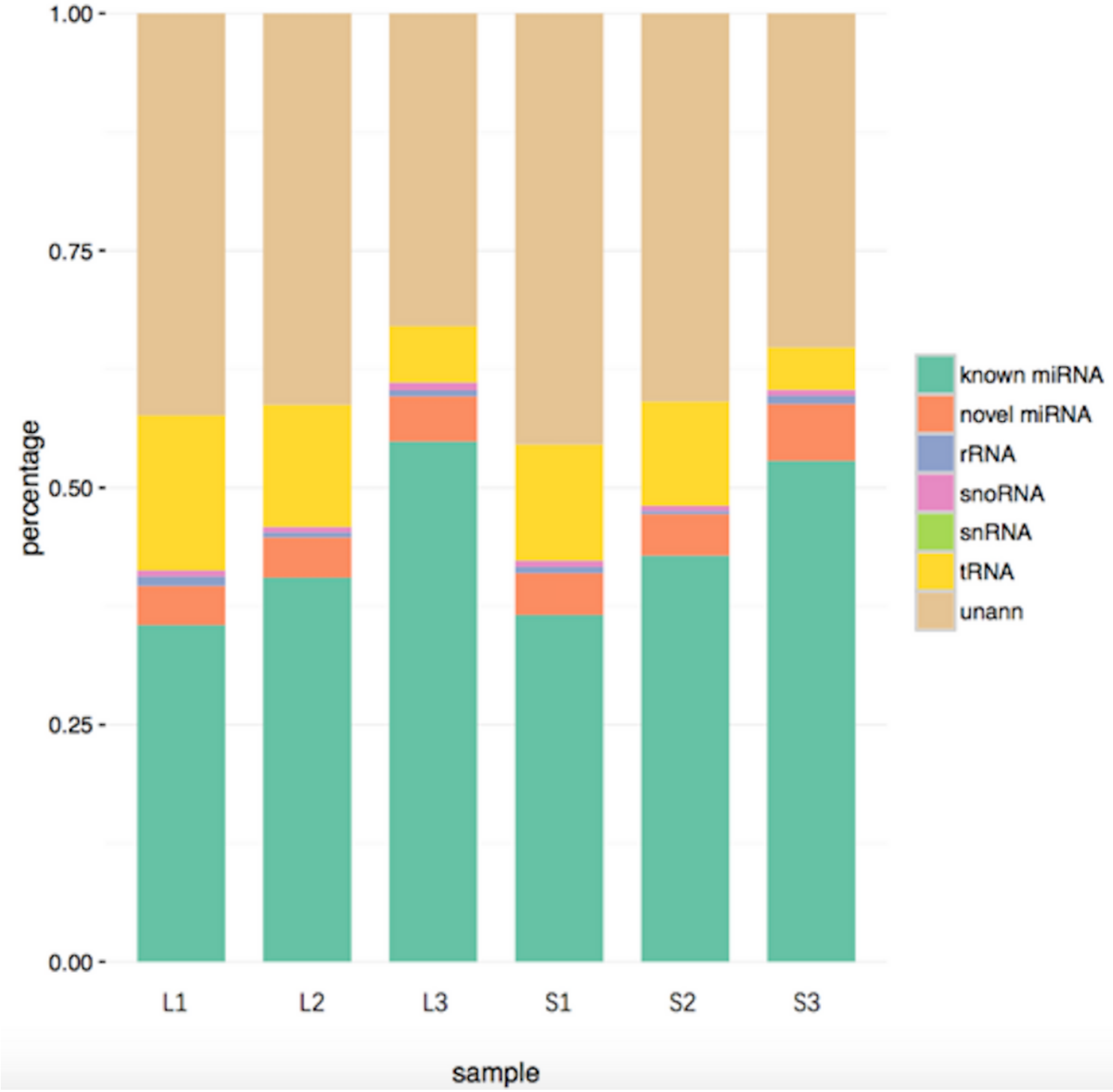

Figure 1

Frequency of small RNAs in tail fat tissues of the LTH and STH sheep breeds. The proportion of expressed adipose tissues small RNAs identical to LTH and STH sheep breed: i) the known miRNAs are shaded light green, ii) the novel miRNAs are shaded red, iii) repeat-associated RNA sequences are shaded blue (including rRNA, snoRNAs, and snRNAs), iv) tRNAs are shaded yellow, and v) the proportion of mapped but unclassified sequences is shaded brown.

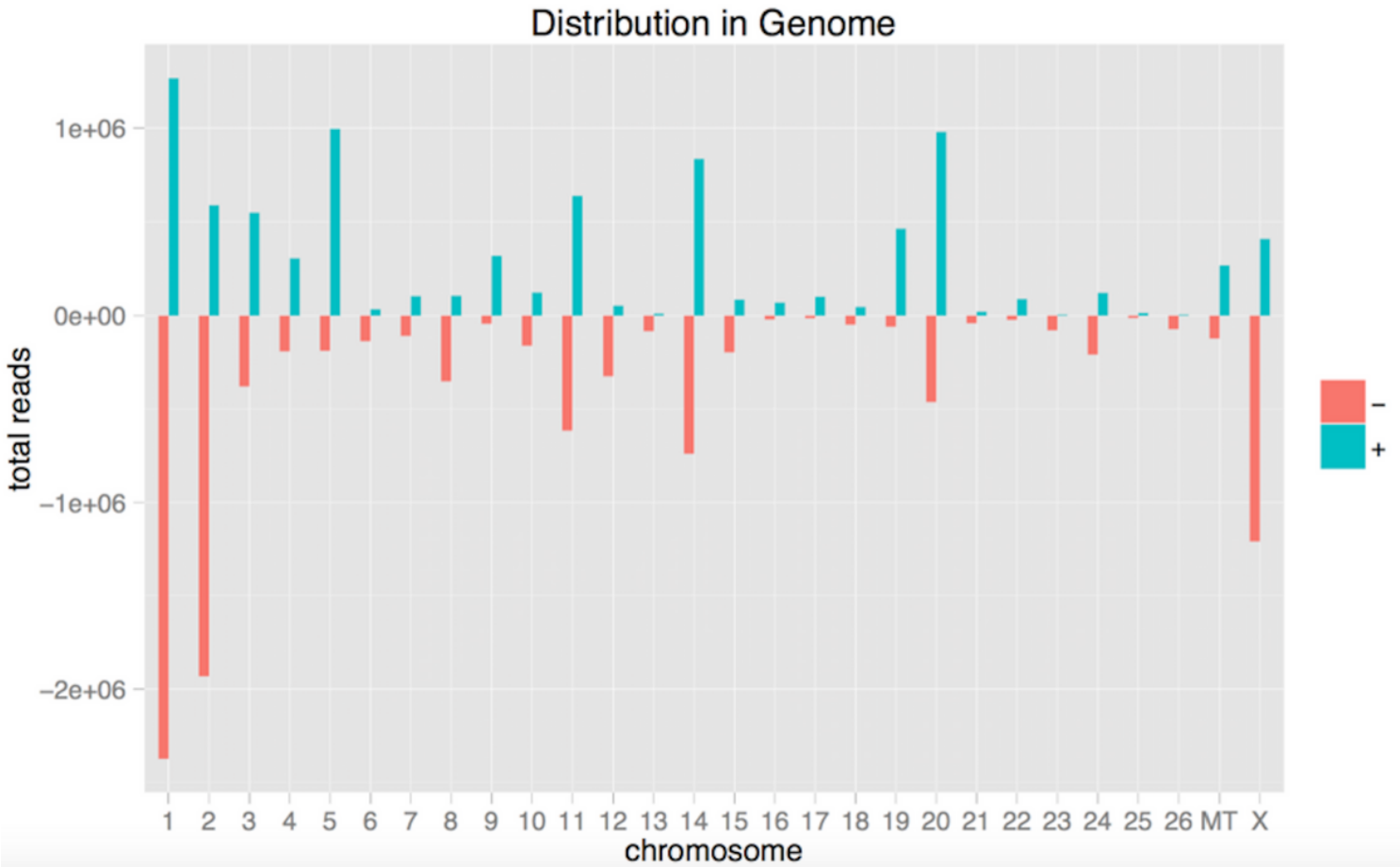

Figure 2

Small RNAs could be mapped to the sheep genome

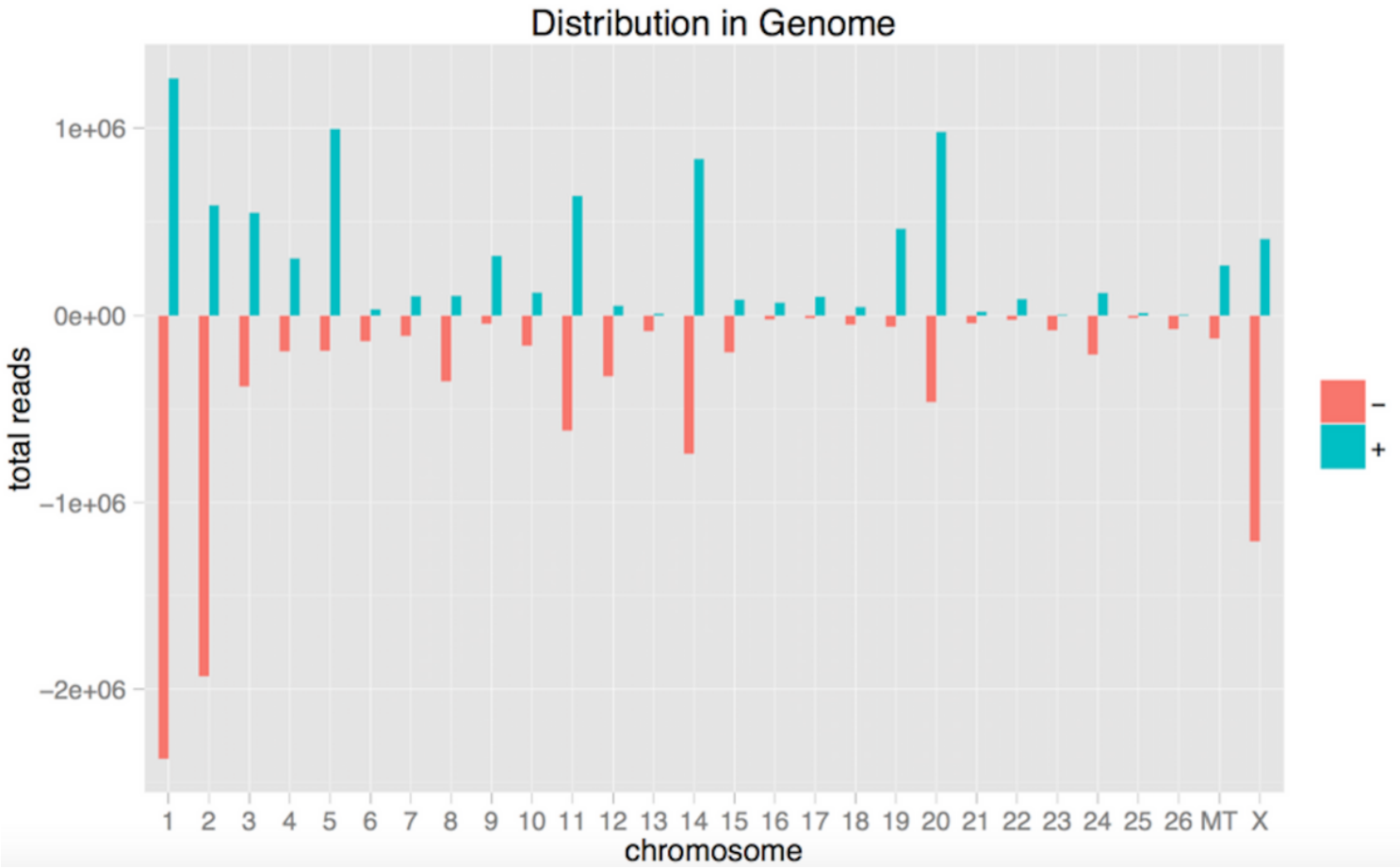

Figure 2

Small RNAs could be mapped to the sheep genome

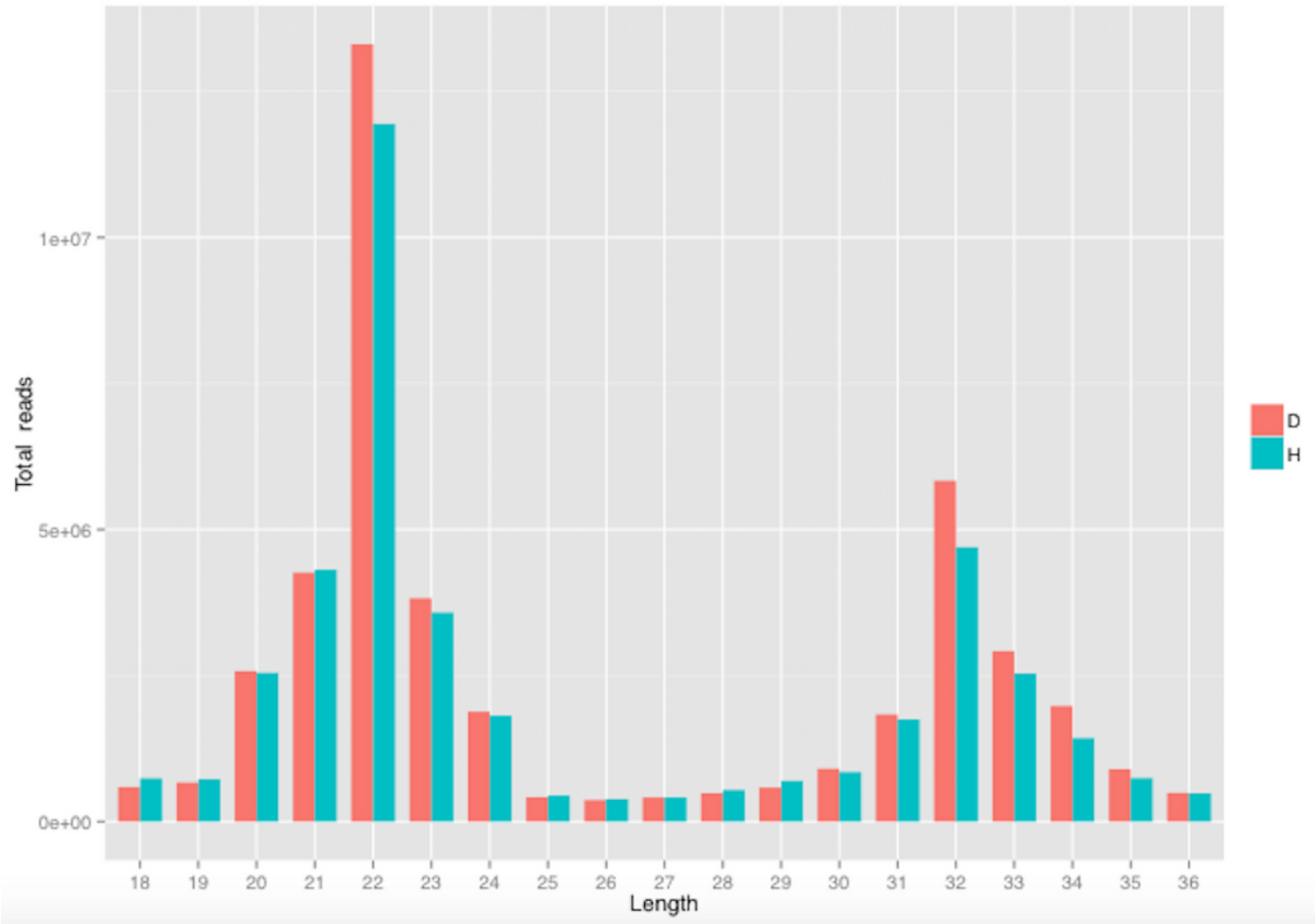

Figure 3

Frequencies and lengths of tail fat tissues sequence reads of the LTH and STH. The proportion (%) of different lengths of sequence reads that aligned to the human miRNAs. The number above each bar indicates the total number of reads with corresponding size.

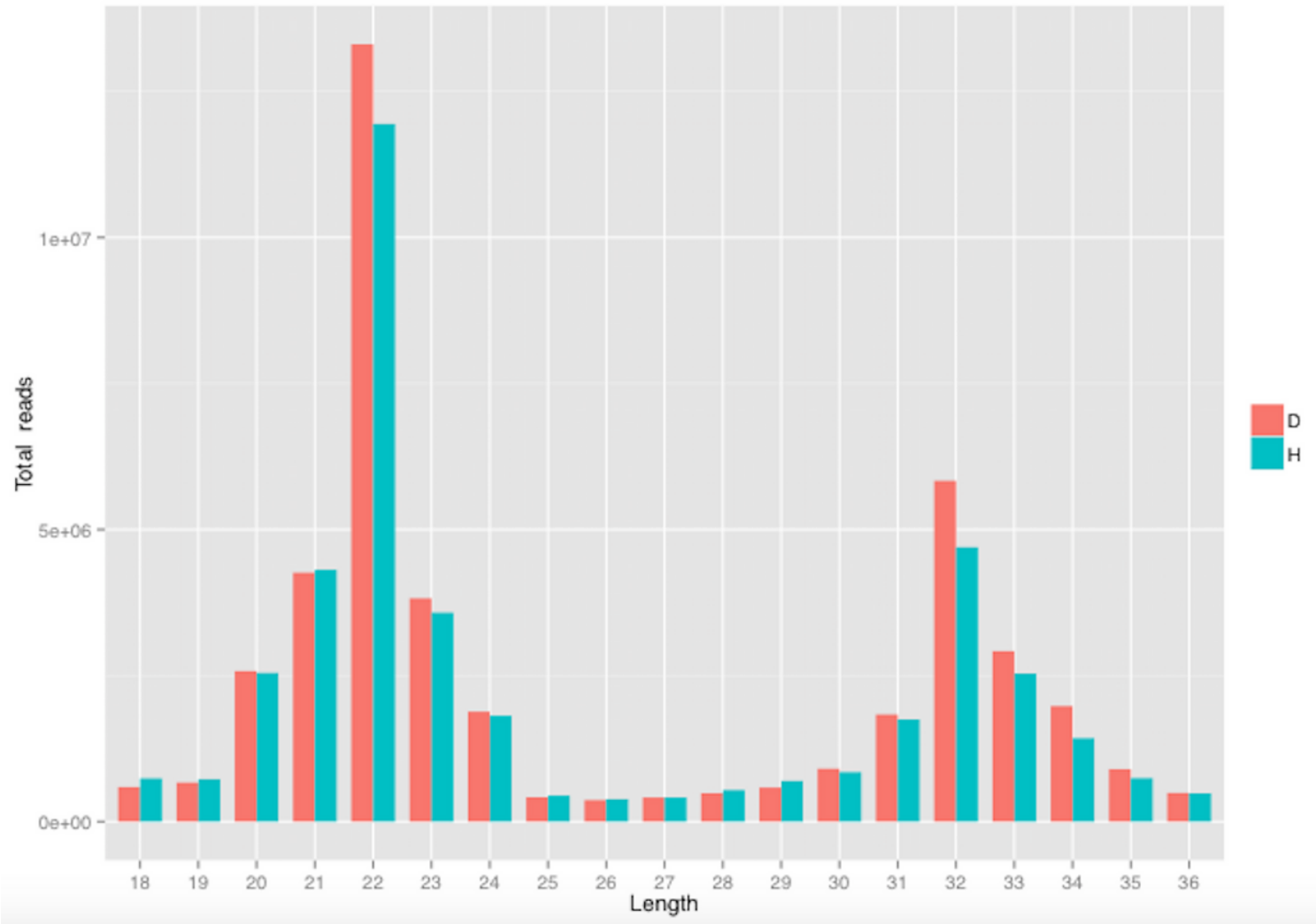

Figure 3

Frequencies and lengths of tail fat tissues sequence reads of the LTH and STH. The proportion (%) of different lengths of sequence reads that aligned to the human miRNAs. The number above each bar indicates the total number of reads with corresponding size.

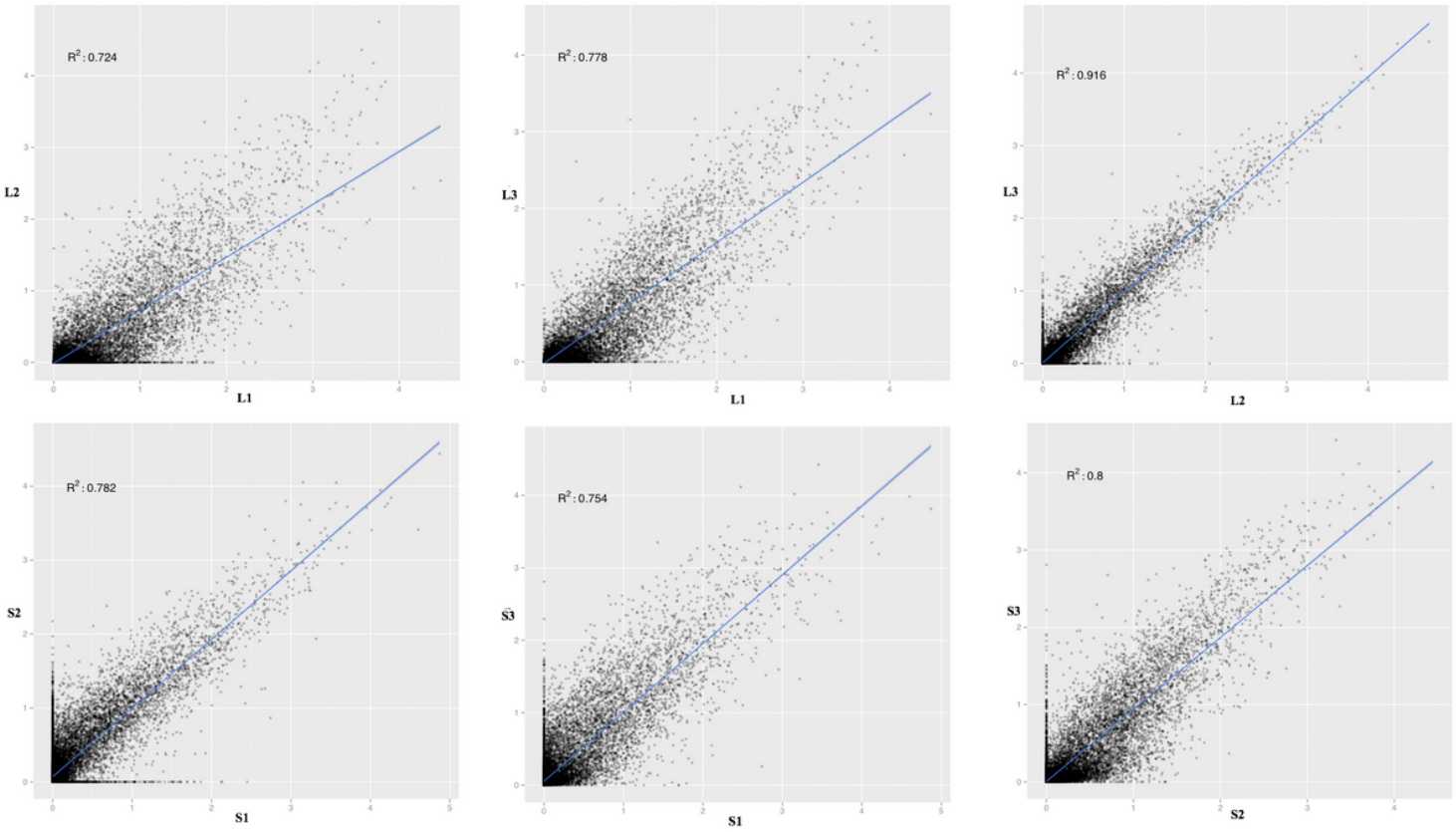

Figure 4

The scatter plot for global expression between samples; the Pearson correlation coefficient is shown.

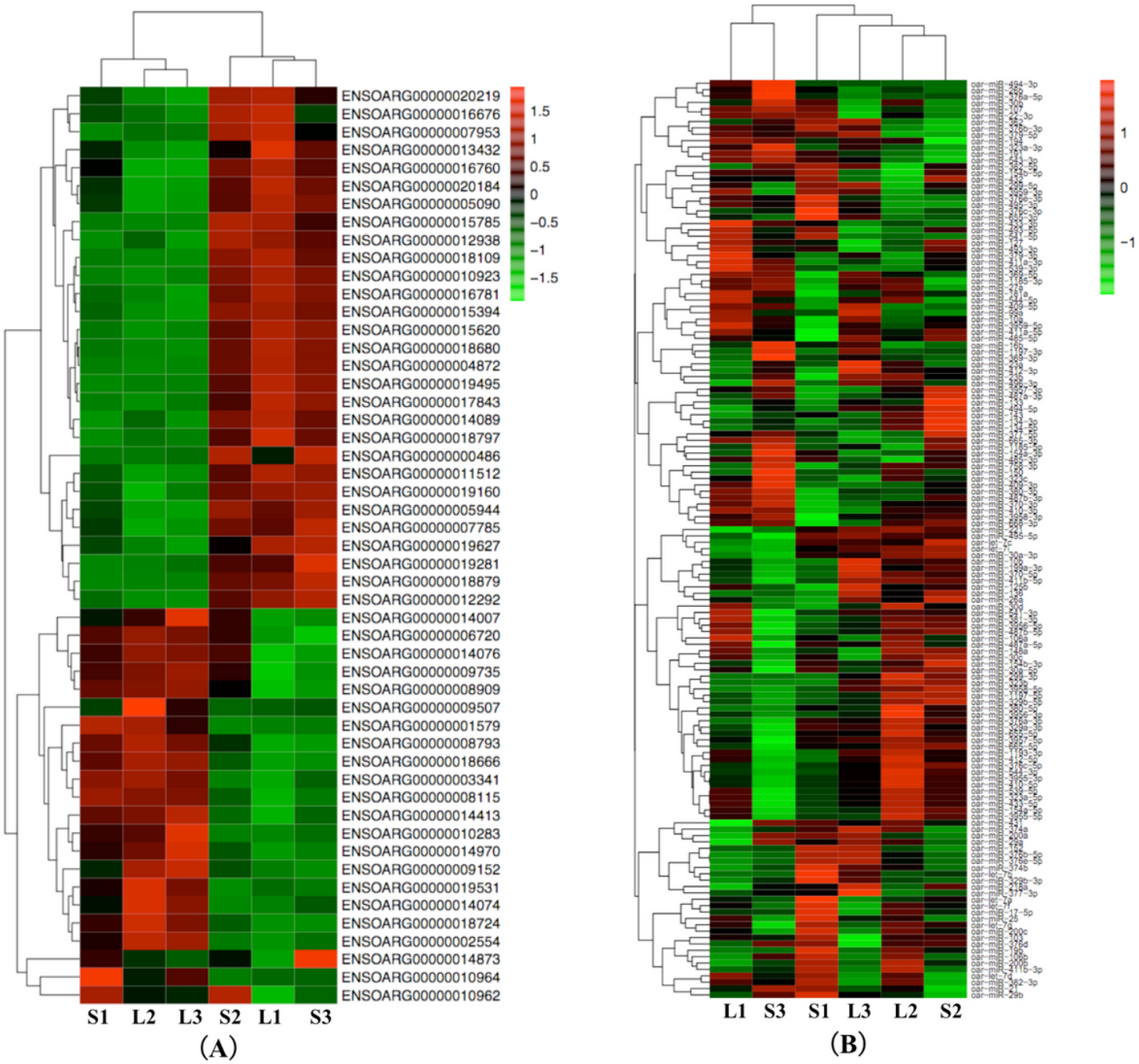

Figure 5

MiRNA and mRNA expression profiles of sheep tail adipose tissues. Heat map and hierarchical clustering showing the differentially expressed mRNAs (A) and miRNAs (B) among samples from LTH and STH breeds.

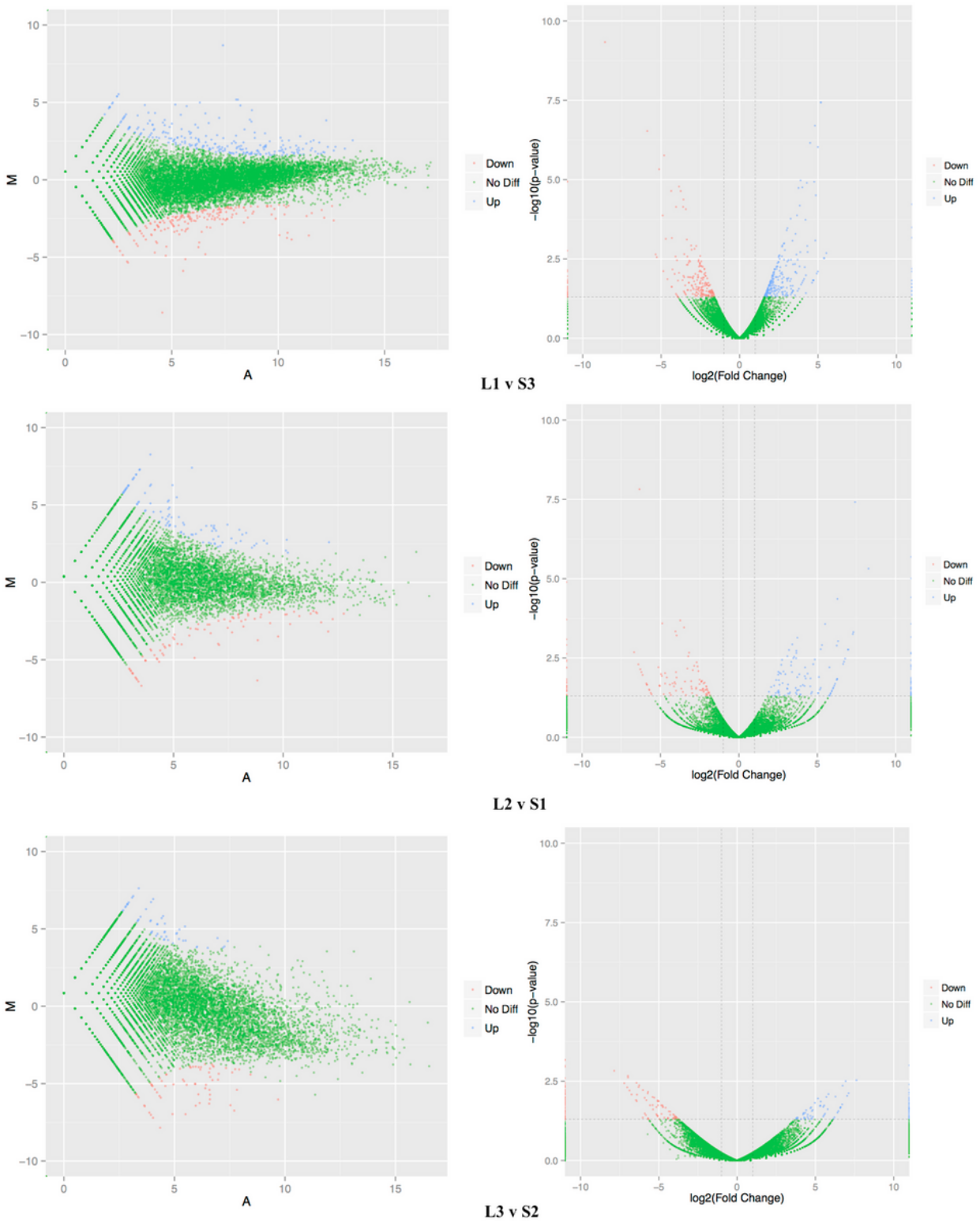

Figure 6

Volcano plots for all the genes in each comparison. The red and blue dots indicate that up- and down-regulated DEGs were significant at p values less than 0.01.

Supplementary Files

This is a list of supplementary files associated with this preprint. Click to download.

- TableS1.xlsb
- TableS1.xlsb
- TableS10.xlsx
- TableS10.xlsx
- TableS2.xlsx
- TableS2.xlsx
- TableS3.xlsx
- TableS3.xlsx
- TableS4.XLSX
- TableS4.XLSX
- TableS5.xlsx
- TableS5.xlsx
- TableS6..xlsx
- TableS6..xlsx
- TableS7..xlsx
- TableS7..xlsx
- TableS8.docx
- TableS8.docx
- TableS9.docx
- TableS9.docx